Supplementary Information

Green Mechanochemical Activation for Acid-free Recovery of Valuable Metals from Spent Lithium-ion Battery Sulfide Residue

He Li [a, b], Kaixuan Sun [a, d], Yadong Ning [a], Guangye Wei [*, a], Jingkui Qu [*, a, c], Caixia Lv [a], Zhihui Yu [a]

[a] National Engineering Research Center of Green Recycling for Strategic Metal Resources, Institute of Process Engineering, Chinese Academy of Sciences, Beijing 100190, China.

[b] University of Chinese Academy of Sciences, Beijing 100049, China.

[c] China-Mongolia Belt and Road Joint Laboratory of Mineral Processing Technology, Inner Mongolia Academy of Science and Technology, Hohhot, 010000, China.

[d] College of Environment and Chemical Engineering, Dalian University, Dalian 116622, China.

[*]**Corresponding author:**

[*]E-mail: gywei@ipe.ac.cn (Guangye Wei), jkqu@ipe.ac.cn (Jingkui Qu)

Number of pages: 22

Number of figures: 14

Number of tables: 13

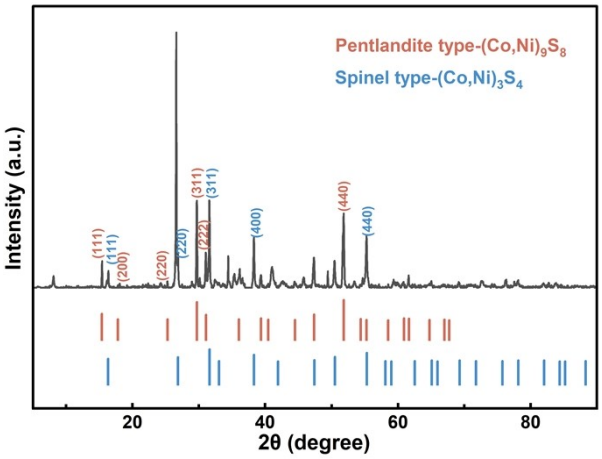

Figure S 1. XRD pattern of sulfide residue

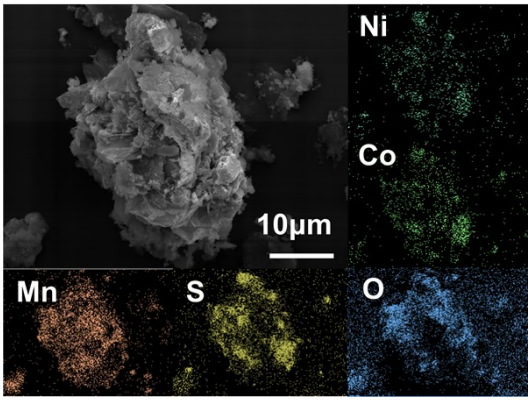

Figure S 2. SEM analysis of sulfide residue particle

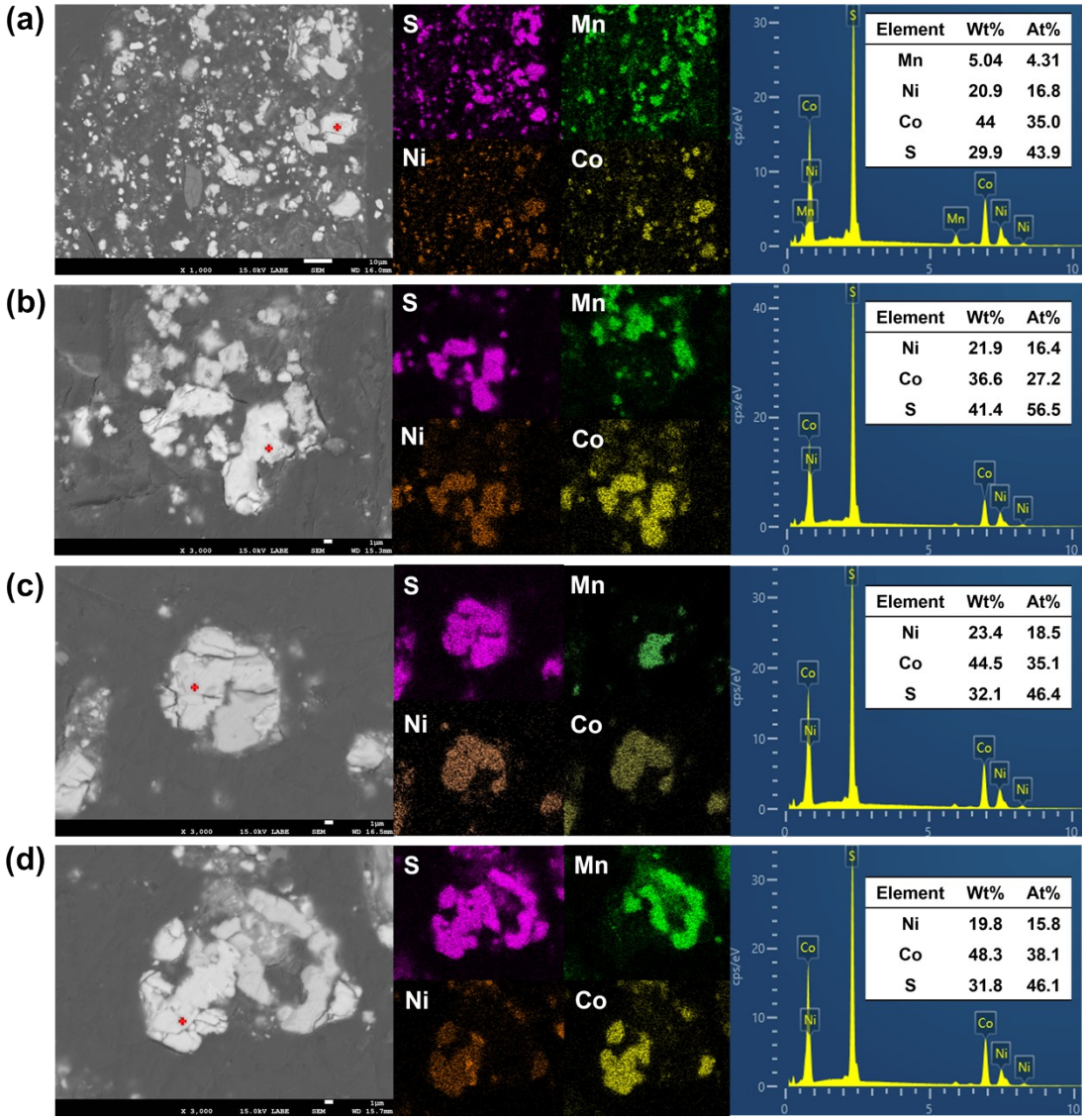

Figure S 3 SEM-DES analysis of sulfide residue particle using resin embedding of cross-section

Text S1

Pentlandite exhibits a cubic cell with Fm3m symmetry and a chemical formula of M_9S_8. The structure consists of approximately close-packed alternating layers of sulfur and metal atoms. The cations are distributed across 32 tetrahedral sites in a cube cluster arrangement, each bonded to 4 sulfur anions, and 4 octahedral sites joining the cube clusters, each bonded to 6 sulfur anions. The tetrahedral cation sites of neighbouring cube clusters have relatively short interatomic distances, indicating some delocalisation of d-electrons between these atoms [1]. Of the 32 sulfur atoms, 24 occupy 5-coordinate "face capping" sites, capping the faces of the cube clusters, and the remaining 8 sulfur anions occupy 4-coordinate sites "linking" the cube clusters [2].

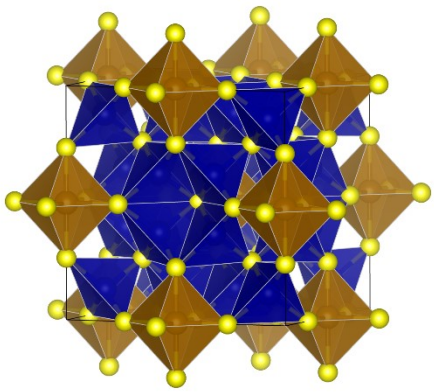

Figure S 4. Structure of pentlandite

Text S2

The effects of ball milling speed and ball to material ratio on the leaching rates of various metals is shown in Figure S 4. As the ball milling speed and ball to material ratio increased, the leaching rate of valuable metals gradually increased, while the leaching rate of impurity iron decreased to almost no leaching, and the leaching rates of copper and aluminum also decreased. Therefore, the optimal conditions are selected as a ball milling speed of 400 rpm and a ball to material ratio of 10:1.

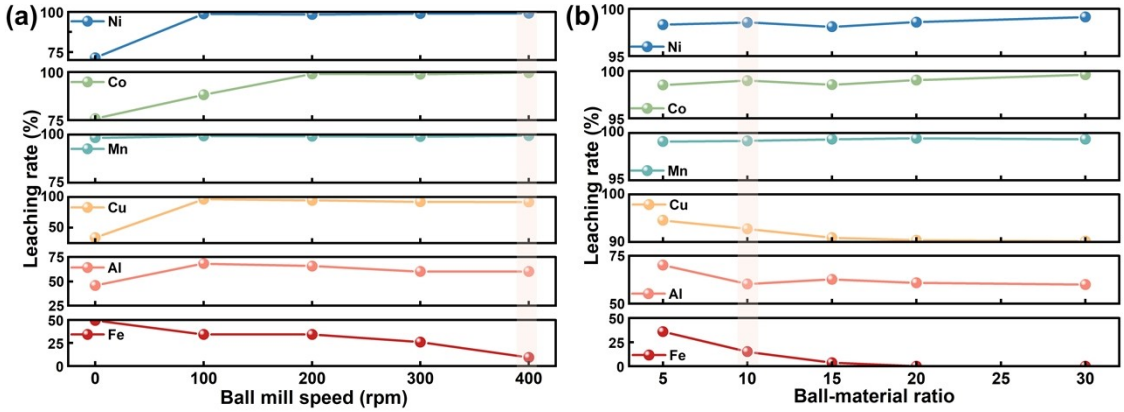

Figure S 5. The effect of (a) ball mill speed, (b) ball to material ratio on metal leaching rates.

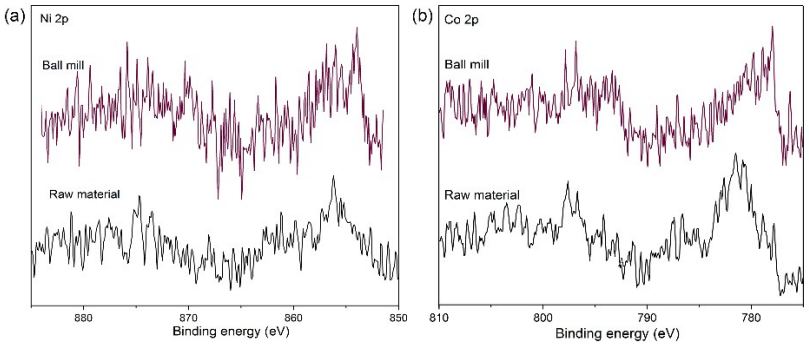

Figure S 6. XPS spectra of (a) Ni 2p, (b) Co 2p of raw material and mechanical activation.

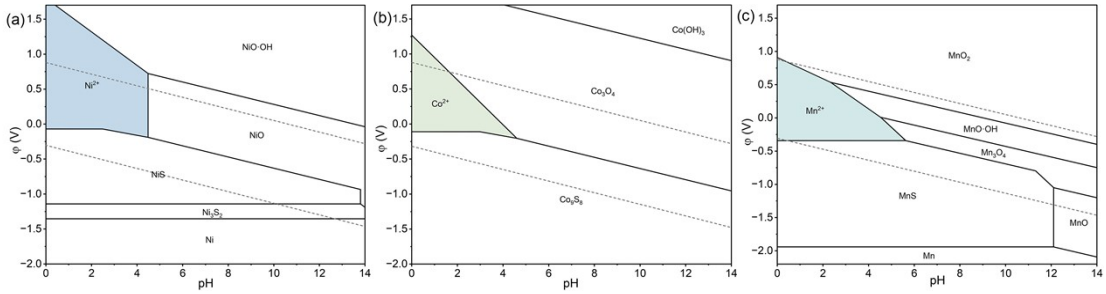

Figure S 7. E-pH diagrams of (a) Ni, (b) Co, (c) Mn under 130 ℃, 0.5 MPa

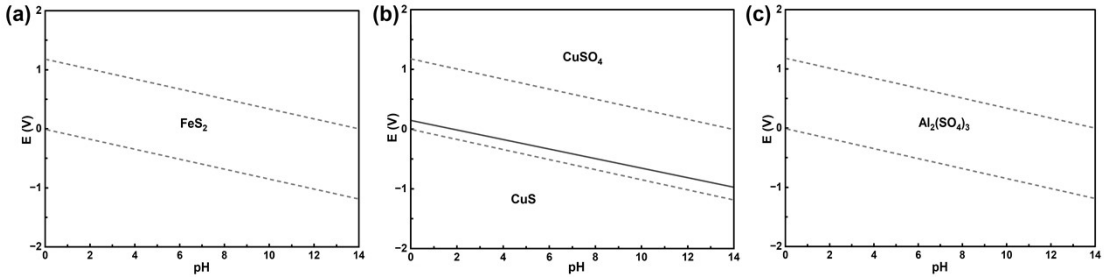

Figure S 8. E-pH diagrams of (a) Fe, (b) Cu, (c) Al under 130 ℃, 0.5 MPa

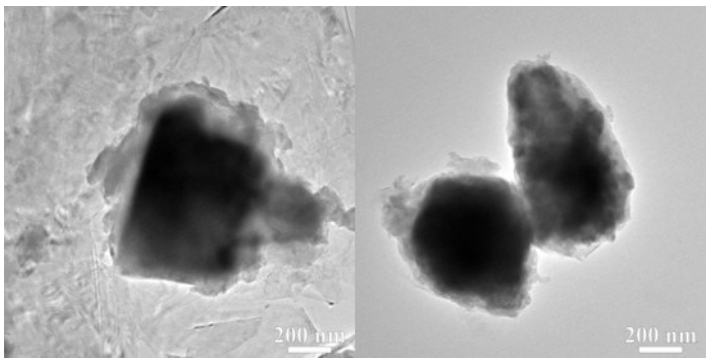

Figure S 9 TEM images of activated material

Table S 1 Composition of sulfide residue

Element	Ni	Co	Mn	Fe	Cu	Al	C	S
wt%	12.95	15.95	17.33	0.61	0.91	1.16	12.4	10.7

The interplanar spacing of the mechanically activated material decreases, and the crystallite size is substantially reduced. The calculation results are shown in Table S2. On the (111) crystal plane, the microstrain (ε) of pentlandite type-$(Co,Ni)_9S_8$ increases by 0.44%, while that of spinel type-$(Co,Ni)_3S_4$ increases by 0.24%, indicating a strong effect of mechanical activation.

Table S 2. Lattice data of sulfide residue

	2θ (degree)	(h k l)	d (Å)	FWHM	XS (nm)	ε (%)
Spinel type-$(Co,Ni)_3S_4$						
Before MA	16.241	111	5.4728	0.115	681	0.3517
After MA	16.299	111	5.4469	0.196	400	0.5972
Before MA	31.470	311	2.8410	0.146	552	0.2261
After MA	31.500	311	2.8353	0.416	194	0.4175
Before MA	55.140	440	1.6644	0.233	376	0.1947
After MA	55.180	440	1.6634	0.547	154	0.2796
Pentlandite type-$(Co,Ni)_9S_8$						
Before MA	15.299	111	5.7902	0.092	851	0.2350
After MA	15.319	111	5.7745	0.208	376	0.6748
Before MA	29.590	311	3.0185	0.138	581	0.2281
After MA	29.639	311	3.0131	0.353	227	0.5822
Before MA	51.700	440	1.7674	0.240	359	0.2161
After MA	51.821	440	1.7654	0.572	151	0.5138
MnS						
Before MA	34.308	200	2.6137	0.084	966	0.1187
After MA	34.262	200	2.6133	0.253	321	0.3581
Before MA	49.319	220	1.8462	0.086	993	0.0817
After MA	49.338	220	1.8473	0.432	243	0.3338

66 Table S 3 Lattice data of different activation time of sulfide residue

$(Co,Ni)_3S_4$	311	d (Å)	FWHM	D (nm)
t=0	31.578	2.8318	0.166	625
t=20	31.516	2.8363	0.232	393
t=60	31.519	2.8361	0.223	415
t=90	31.506	2.8372	0.230	398
t=120	31.528	2.8353	0.245	230
t=180	31.534	2.8358	0.279	360
t=240	31.584	2.8358	0.356	260
$(Co,Ni)_3S_4$	440	d (Å)	FWHM	D (nm)
t=0	55.268	1.6628	0.290	330
t=20	55.169	1.6634	0.316	299
t=60	55.182	1.6631	0.235	420
t=90	55.162	1.6637	0.237	430
t=120	55.174	1.6633	0.306	310
t=180	55.203	1.6629	0.405	220
t=240	55.376	1.6596	0.599	140
$(Co,Ni)_9S_8$	311	d (Å)	FWHM	D (nm)
t=0	29.689	3.0068	0.158	669
t=20	29.622	3.0102	0.162	647
t=60	29.635	3.0119	0.176	568
t=90	29.616	3.0138	0.192	500
t=120	29.629	3.0126	0.202	467
t=180	29.637	3.0134	0.240	440
t=240	29.715	3.0057	0.256	400
$(Co,Ni)_9S_8$	440	d (Å)	FWHM	D (nm)
t=0	51.842	1.7621	0.257	374
t=20	51.744	1.7652	0.294	319
t=60	51.770	1.7644	0.310	301

t=90	51.749	1.7651	0.324	287
t=120	51.756	1.7649	0.339	273
t=180	51.779	1.7652	0.427	210
t=240	51.838	1.7628	0.438	200
MnS	200	d (Å)	FWHM	D (nm)
t=0	34.363	2.6076	0.08	>1000
t=20	34.294	2.6127	0.084	>1000
t=60	34.304	2.6119	0.116	>1000
t=90	34.312	2.6114	0.106	>1000
t=120	34.314	2.6112	0.143	811
t=180	34.331	2.6112	0.216	520
t=240	34.406	2.6070	0.258	400
MnS	220	d (Å)	FWHM	D (nm)
t=0	49.375	1.8442	0.089	>1000
t=20	49.313	1.8464	0.106	>1000
t=60	49.300	1.8469	0.121	>1000
t=90	49.305	1.8467	0.115	>1000
t=120	49.316	1.8463	0.188	549
t=180	49.338	1.8467	0.294	330
t=240	49.397	1.8445	0.329	290

67

Text S3

After oxygen-pressure water leaching, iron is largely removed from the solution due to oxidation and precipitation under the applied conditions. As a result, the main residual impurities in the leachate are Cu and Al, while Fe remains at a very low level. The leachate pH is approximately 2, and the concentrations of the dissolved species are summarized

Table S 4. Elements concentration of leachate

Element	Ni	Co	Mn	Fe	Cu	Al	P
Content (g/L)	13.38	16.60	21.94	0.04	0.81	0.33	0.028

Considering selectivity, cost, and compatibility with downstream processes, manganese powder cementation was adopted for copper removal. Industrial-grade manganese powder (100 mesh) is economically feasible and does not introduce foreign impurity elements into the system. As shown in Fig. 2a, at $n(Mn):n(Cu^{2+})=1.4$, a Cu removal efficiency of 91% was achieved, and loss rate of Ni, Co and Mn were 0.02%, 0.14%, and 0.002%, respectively. Further optimization showed that adjusting the solution pH to 2.9 increased the Cu removal efficiency to 96.36%, while maintaining very low losses of Ni (0.028%), Co (0.142%), and Mn (0.019%). The final solution pH after cementation was 3.8-3.9. Increasing temperature improved selectivity but significantly reduced Cu removal efficiency (<80%). Therefore, ambient temperature was selected as the optimal condition. XRD analysis of the precepitation confirmed the formation of sponge copper with a purity of approximately 95%, containing only trace amounts of Fe and Co.

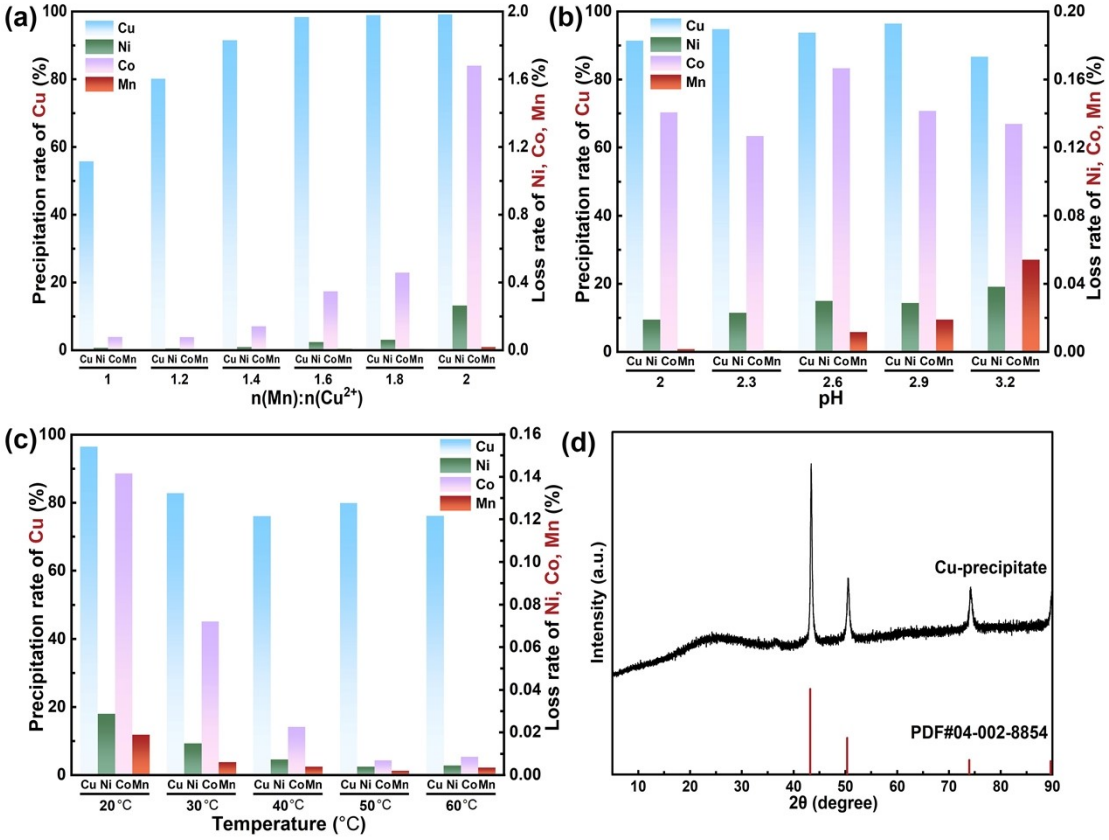

Figure S 10. Effect of (a) n(Mn):n(Cu^{2+}), (b) pH, (c) temperature on removal of Cu, (d) XRD pattern of Cu-precipitation.

Subsequently, aluminum was removed from the Cu-free leachate by phosphate precipitation. At a molar ratio of n(Na_3PO_4):n(Al^{3+})=1, an Al removal efficiency of 95.3% was achieved, with minimal losses of Ni (0.027%), Co (0.033%), and Mn (0.045%), and the lowest residual phosphorus concentration in solution. Increasing temperature did not significantly enhance Al removal but increased valuable metal losses; therefore, ambient temperature was selected. As the solution pH was already within the effective range for Al precipitation, no further pH adjustment was required. Under these conditions, residual Fe was also completely removed, and the resulting precipitate showed no distinct peaks.

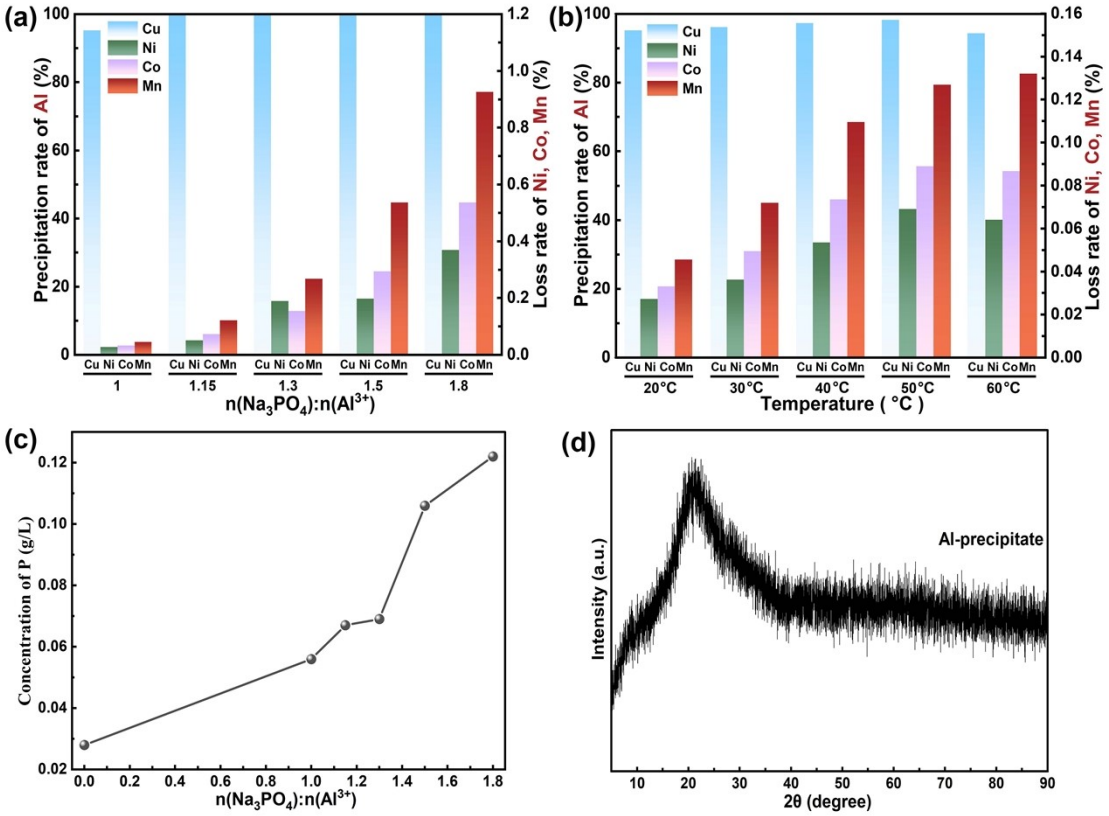

Figure S 11. Effect of (a) $n(Na_3PO_4):n(Al^{3+})$, (b) temperature on the removal of Al, (c) Concentration of P left in the leachate, (d) XRD pattern of Al-precipitation.

Overall, the combined Mn cementation for Cu removal and phosphate precipitation for Al removal resulted in a total valuable metal loss of less than 0.3%. The purified leachate composition, summarized in Table R2, meets the purity requirements for the subsequent synthesis of ternary lithium-ion battery precursors. All purification experiments and corresponding data have been added to the Supporting Information.

Table S 5. Element concentration of leachate after impurities removal

Element	Ni	Co	Mn	Fe	Cu	Al	P
Content (g/L)	13.24	16.16	22.54	-	0.009	0.006	0.05

Techno-economic analysis

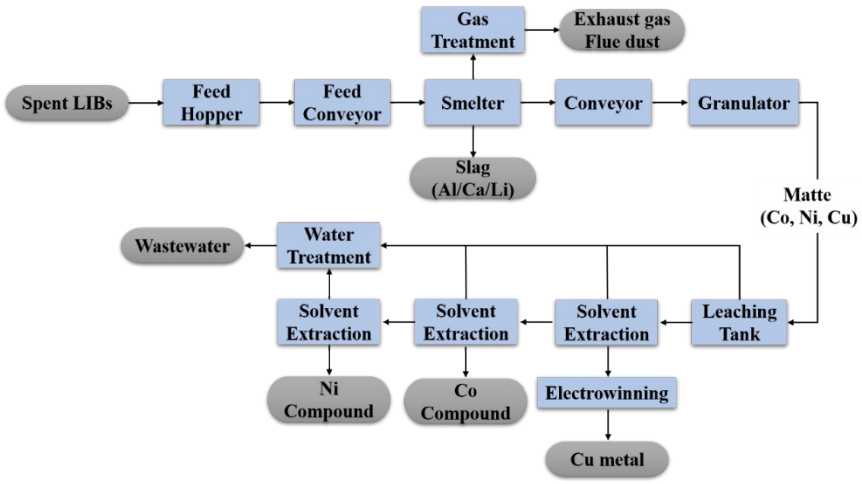

Figure S 12. Process diagram of a generic pyrometallurgical recycling process.

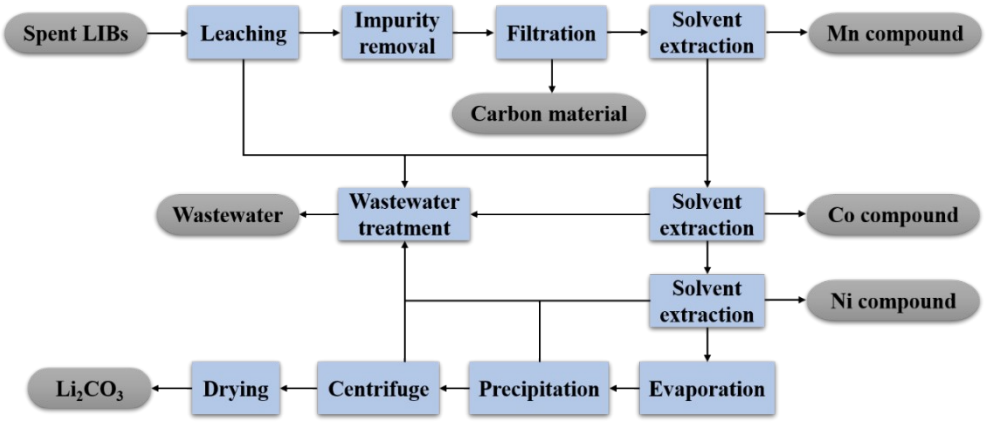

Figure S 13. Process diagram of a generic hydrometallurgy recycling process

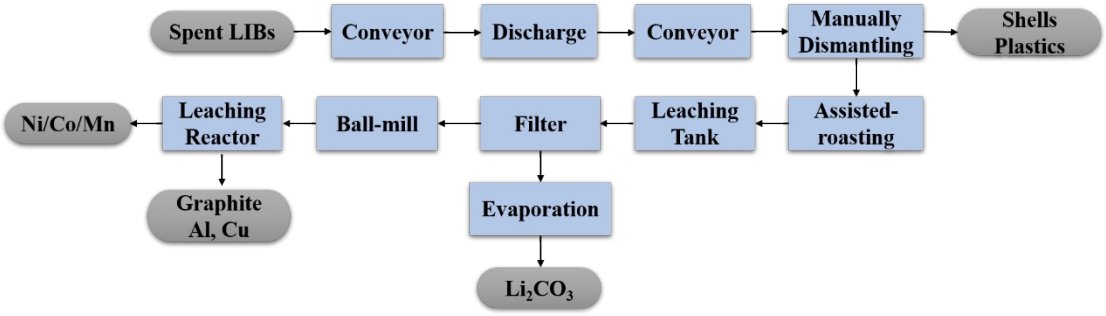

Figure S 14. Process diagram of pyro-hydro recycling process

119 Table S 6.Price of materials of different recycling methods.

The price of materials			
No.	Item	Market price ($\$\cdot kg^{-1}$)	Quantity (kg)
Generic hydro process			
1	Ammonium Hydroxide	0.53	0.03
2	Hydrochloric Acid	0.57	0.01
3	Hydrogen Peroxide	1.46	0.37
4	Sodium Hydroxide	0.45	0.56
5	Sulfuric Acid	0.08	1.08
6	Soda Ash	0.14	0.02
Generic pyro process			
7	Limestone	0.13	0.3
8	Sand	0.05	0.15
9	Hydrochloric Acid	0.57	0.21
10	Hydrogen Peroxide	1.46	0.06
Pyro-hydro process			
11	Oxygen	0.2	0.2
12	Industrial Na_2S (>60%)	0.33	0.8
13	Sulfur	0.28	0.06

120

121

122 Table S 7. Cost analysis of different recycling methods.

Cost of generic hydro process		
Main	Note	Cost per kg feed $
Raw materials	$6.01 per kg NCM111 feedstock	6.01
Reagent	Seen Table S6	0.903
Average labor	$34560 for operating labor, management and salary	0.07
Utilities cost	0.088 $/kWh electricity for 34722 kWh/yr	0.035
	0.002 $/gal process water for 1000000 gal/yr	
	0.011 $/MJ natural gas for 2500000 MJ/yr	
Other variable costs	Effluent disposal, packaging and shipping	0.15
Maintenance	5% of plant cost	0.2
Other fixed costs	Taxes, insurances, rents, environmental charges	0.42
Annualized capital cost	Fixed capital investment, plant costs	1.21
	Total	8.52
Cost of generic pyro process		
Main	Note	Cost per kg feed $
Raw materials	$6.01 per kg NCM111 feedstock	6.01
Reagent	Seen Table S6	0.2538
Average labor	$34560 for operating labor, management and salary	0.07
Utilities cost	0.088 $/kWh electricity for 1300000kWh/yr	0.1149
Other variable costs	Effluent disposal, packaging and shipping	0.42
Maintenance	5% of plant cost	0.37
Other fixed costs	Taxes, insurances, rents, environmental charges	0.42
Annualized capital cost	Fixed capital investment, plant costs	2.28
	Total	8.98
Cost of pyro-hydro process		
Main	Note	Cost per kg feed $
Raw materials	$6.01 per kg NCM111 feedstock	6.01
Reagent	Seen Table S6	0.3208

Average labor	$34560 for operating labor, management and salary	0.07
Utilities cost	0.088 $/kWh electricity for 1300000kWh/yr	0.09
Other variable costs	Effluent disposal, packaging and shipping	0.13
Maintenance	5% of plant cost	0.11
Other fixed costs	Taxes, insurances, rents, environmental charges	0.42
Annualized capital cost	Fixed capital investment, plant costs	0.68
	Total	7.41

123

124

125 Table S 8. Revenue of different process.

Revenue of hydro process		
No.	Item	Revenue
1	Li_2CO_3	3
2	Co^{2+} in product	6.31
3	Ni^{2+} in product	2.1
4	Mn^{2+} in product	0.37
5	Graphite	0.06
Revenue of pyro process		
No.	Item	Revenue
1	Li_2CO_3	1.5
2	Copper	0.07
3	Co^{2+} in product	6.12
4	Ni^{2+} in product	2.04
Revenue of pyro-hydro process		
No.	Item	Revenue
1	Li_2CO_3	3.8
2	Co^{2+} in product	7.05
3	Ni^{2+} in product	2.53
4	Mn^{2+} in product	0.54
5	Graphite	0.06

126

127

128 Table S 9. Total emissions of different methods

Total Emission in g per kg BM	Hydro	Pyro	Pyro-hydro
VOC	0.394	0.181	0.062
CO	1.324	0.718	0.245
NO_x	2.353	1.469	0.531
PM_{10}	0.191	0.195	0.107
$PM_{2.5}$	0.138	0.105	0.049
SO_x	3.098	1.086	0.671
BC	0.025	0.017	0.002
OC	0.042	0.017	0.005
CH_4	4.975	2.718	1.138
N_2O	0.043	0.033	0.017
CO_2	1800	2804	681
CO_2 (w/C in VOC & CO)	1803	2806	681
GHGs	1963	2896	835

129

130

According to the national standard document (GBT 25323-2023) "The norm of energy consumption per unit production of non-ferrous heavy metals metallic enterprises". The energy consumption per unit product of the newly built nickel smelting plant (1887.71 kWh t^{-1} NSC^{-1}) is selected as the energy consumption for the production of high nickel matte from NSC. According to the national standard document (GBT51388-2020) "Standard for process design of nickel plants", the steam consumption should be less than 3950 kg t^{-1} $NiSO_4^{-1}$ and the power consumption should be less than 372 kWh t^{-1} $NiSO_4^{-1}$ in the production of nickel sulfate from high nickel matte by pressure leaching. After conversion, the energy consumption of pressure leaching is 1336.61 kWh t^{-1} NSC^{-1}. Compared to oxygen-pressure water leaching, heating the slurry is the main energy consumption in the process, $E = cm\Delta t \cdot 0.2776 = 930\ kWh\ t^{-1}NSC^{-1}$, which is 534 kWh t^{-1} for producing $NiSO_4$. With the addition of 372 kWh t^{-1} $NiSO_4^{-1}$ electricity consumption, the energy consumption is 906 kWh t^{-1}. Energy for ball milling is 832 kWh t^{-1} [3].

Table S 10. Comparison of high-pressure acid leaching and mechanochemical-leaching

Process		Energy consumption (kWh t^{-1} NSC^{-1})	GHG emissions (tCO_2 t^{-1} NSC^{-1})	Materials cost (\$ t^{-1})
High-pressure acid leaching	Pyrometallurgy	1887	1.244	143.27
	High oxygen-pressure leaching	1336	0.762	
Mechanochemical -leaching	Mechanochemical activation	830	0.473	27.92
	Oxygen-pressure water leaching	906	0.516	

Life-cycle analysis

LCI data:

Table S 11. LCI data of hydrometallurgy recycle process

Input	Black mass	1	kg
	Sulfric acid	1.628	Kg
	Water	9.72	kg
	30% H_2O_2	0.13	Kg
	Kerosene	7.94	kg
	Extraxtant	3.63	kg
	NaOH	1	Kg
	$NH_3{\cdot}H_2O$	0.14	Kg
	Na_2CO_3	0.3	kg
Energy	Electricity	14	kWh
Output	Cathode material	0.75	kg
	Slag	0.31	kg
	Waste water	6	kg

Table S 12. LCI data of pyrometallurgy recycle process

Input	Black mass	1	kg
	Sulfric acid	1.34	Kg
	Water	12.8	kg
	Coal	0.78	Kg
	NaOH	1.136	Kg
	$NH_3{\cdot}H_2O$	0.15	Kg
	30% H_2O_2	0.22	kg
	Na_2CO_3	0.23	kg
Energy	Electricity	12.2	kWh
Output	Cathode material	0.71	kg
	Slag	0.078	kg
	Waste water	13.3	kg

Table S 13. LCI data of pyro-hydro recycle process

Input	Black mass	1	kg
	Sulfur	0.065	Kg
	Water	13	kg
	Sodium sulfide	0.48	Kg
	NaOH	0.6	Kg
	$NH_3{\cdot}H_2O$	0.13	Kg
	Mn powder	0.0052	kg
	Na_3PO_4	0.0013	kg
Energy	Electricity	10.6	kWh
Output	Cathode material	0.78	kg

	Slag	0.12	kg
	Waste water	5	kg

References

1 A. Mikuła, J. Dąbrowa, A. Kusior, K. Mars, R. Lach and M. Kubowicz, *Dalton Trans.*, 2021, **50**, 9560–9573.

2 Z. E. Pettifer, J. S. Quinton, W. M. Skinner and S. L. Harmer, *Applied Surface Science*, 2020, **504**, 144458.

3 Q. Zhang, X. Zheng, W. Lv, M. He, W. Yan, W. Gao, P. Ning, H. Cao and Z. Sun, *Nat Commun*, 2025, **16**, 4687.